Background pycnocline depth constrains future Ocean Heat Uptake Efficiency

Article

Published Version

It is advisable to refer to the publisher's version if you intend to cite from the work. See Guidance on citing.

www.reading.ac.uk/centaur

CentAUR

Geophysical Research Letters®

Author Contributions:

Conceptualization: Emily Newsom, Laure Zanna, Jonathan Gregory
Data curation: Emily Newsom
Formal analysis: Emily Newsom, Laure Zanna
Funding acquisition: Laure Zanna
Methodology: Emily Newsom
Validation: Emily Newsom
Visualization: Emily Newsom
Writing – original draft: Emily Newsom
Writing – review & editing: Emily Newsom, Laure Zanna, Jonathan Gregory

Background Pycnocline Depth Constrains Future Ocean Heat Uptake Efficiency

Emily Newsom[1] ![ORCID]**, Laure Zanna[1]** ![ORCID]**, and Jonathan Gregory[2,3]** ![ORCID]

[1]Courant Institute of Mathematical Sciences, New York University, New York, NY, USA, [2]National Centre for Atmospheric Science, University of Reading, Reading, UK, [3]Met Office Hadley Centre, Exeter, UK

Abstract The Ocean Heat Uptake Efficiency (OHUE) quantifies the ocean's ability to mitigate surface warming through deep heat sequestration. Despite its importance, the main controls on OHUE, and on its two-fold spread across contemporary climate models, remain unclear. We argue that OHUE is primarily controlled by mid-latitude ventilation strength in the background climate, itself related to pycnocline depth and stratification. This hypothesis is supported by a strong correlation between mid-latitude (30–60°) OHUE and the near-global average (60°S–60°N) pycnocline depth in CMIP5 and CMIP6 AOGCMs under RCP85/SSP585, and in a parameter perturbation ensemble of ocean GCM (MITgcm) experiments. This correlation explains about 70% of the CMIP5-6 spread in global OHUE. The relationship provides a pathway toward observationally constraining OHUE, and thus reducing uncertainty in projections of future global climate change and sea level rise.

Plain Language Summary The ocean absorbs most of the excess heat in the climate system. How effectively this process reduces surface warming depends on how deeply this heat is stored in the ocean, which varies widely across contemporary climate models. Our study shows that around 70% of the variation in deep heat storage across models is explained by differences is how water from the mid-latitude surface ocean is transported to deeper ocean layers by ocean currents. This difference can be measured by the stratification of seawater density in the base-state climate, a feature that can be observed in the modern ocean. We show this relationship using a new regional decomposition method. The results of this study can be leveraged with ocean observations to reduce uncertainty in future climate and sea level rise projections.

1. Introduction

The ocean has absorbed around 90% of the excess energy in the climate system during the industrial age (Cheng et al., 2017; Meyssignac et al., 2019). This quantity is not invariant in time, nor across climate models, but is instead set by dynamical ocean processes. How efficiently these processes sequester heat away from the ocean surface partially determines the rate of surface warming. This study aims to better understand what controls this ocean heat sequestration and identify the dominant factor driving its spread across contemporary atmosphere-ocean climate models (AOGCMs).

In practice, the rate of heat uptake relative to a given surface warming is called the Ocean Heat Uptake Efficiency (OHUE, Gregory & Mitchell, 1997; Raper et al., 2002). OHUE is defined as the change in global-mean rate of ocean heat uptake (N, W m^{-2}) per unit change in global surface temperature, here represented by the sea surface temperature (SST), since our study focuses on ocean processes (Newsom et al., 2020):

$$\text{OHUE} \equiv \frac{\text{N}}{\text{SST}}. \tag{1}$$

Over decadal to centennial timescales, the OHUE has around 30%–75% the influence of the global radiative feedback on the rate of surface warming (Kuhlbrodt & Gregory, 2012) and shares the units of a radiative feedback (Wm^{-2} K^{-1}). While OHUE is useful to quantify how ocean processes mitigate surface warming, it is also quite uncertain, ranging by a factor of one to two across AOGCMs (e.g., Figure 2 of this study; Kuhlbrodt & Gregory, 2012).

The drivers of this spread are unclear, in part because the processes that govern OHUE are not fully understood. Past studies have linked the inter-model spread in OHUE to the background strength of the Atlantic Meridional Overturning Circulation, or AMOC (Kostov et al., 2014; Romanou et al., 2017), given a notable correlation

between the background AMOC strength and depth and of heat and passive tracer transport in AOGCMs. An associated correlation between OHUE and the AMOC strength was also demonstrated across a number of different AOGCMs (Winton et al., 2014). Yet, the mechanism linking AMOC to OHUE is not obvious, given that relatively little anthropogenic heat uptake occurs in the North Atlantic (Saenko et al., 2021), as compared to wind-driven subduction regions in the Southern Ocean and mid-latitudes (Kuhlbrodt & Gregory, 2012; Frölicher et al., 2015; Armour et al., 2016; Shi et al., 2018; Zanna, Khatiwala, et al., 2019; Newsom et al., 2020; Cheng et al., 2022).

More recent work instead argues that the correlation of AMOC and OHUE emerges because of their shared dependence on another aspect of the ocean state, for instance, the strength of transient ocean eddies (Saenko et al., 2018), parameterized by the Gent-McWilliams mesoscale eddy diffusivity, κ_{GM} (Gent & McWilliams, 1990) Indeed, OHUE correlates negatively with κ_{GM} across CMIP3 models (Kuhlbrodt & Gregory, 2012). Similarly, Saenko et al. (2018) showed that although decreasing κ_{GM} in an ocean model (NEMO3.4) increased both AMOC strength and OHUE, the latter change was associated with strengthened Southern Ocean ventilation, not AMOC changes.

While these studies convincingly show the influence of κ_{GM} on OHUE, the wider relevance of this influence is hard to discern, given that many other processes affect both Southern Ocean and global heat uptake in addition to ocean eddies (e.g., Exarchou et al., 2015; Lyu et al., 2020; Morrison et al., 2022). For instance, recent work links higher Southern Ocean surface salinity to more efficient ocean heat uptake in CMIP6 models (Liu et al., 2023), consistent with a similar link between Southern Ocean surface salinity and global carbon uptake (Terhaar et al., 2021). Theory also points to the Southern Ocean mean-state wind strength as a key control on the depth of heat uptake under climate forcing (Marshall & Zanna, 2014).

Here we propose a more generalized perspective on OHUE, one not based on singular process such as the AMOC, transient ocean eddies, or Southern Ocean surface salinity or winds. We propose that OHUE will be primarily controlled by the depth and efficiency of ventilation from the mid-latitudes, itself set by many processes and reflected by the depth of the pycnocline (here meaning, the pycnocline between ≈60°N/S), and the distribution of ocean stratification more broadly.

Our reasoning is based on the idea that, as noted above, the majority of global anthropogenic heat and carbon uptake occurs within the mid-latitudes (e.g., Cheng et al., 2022; Frölicher et al., 2015; Zanna, Khatiwala, et al., 2019), much of which enters the interior along sloping isopycnals (Church et al., 1991; Jackett & McDougall, 1997; Morrison et al., 2022; Saenko et al., 2021) akin to a passive tracer (Couldrey et al., 2021; Gregory et al., 2016; Todd et al., 2020; Winton et al., 2013). Conceptually, a deeper subtropical pycnocline would enable isopycnals outcropping in the mid-latitudes to penetrate more deeply into the interior ocean, enabling deeper along-isopycnal heat subduction under anthropogenic forcing. This concept is depicted schematically in Figure 1, which illustrates the differences in mid-latitude heat penetration between a state with a deep pycnocline to one with a shallow pycnocline. We label these the "High OHUE" and "Low OHUE" states, respectively.

Critically, we propose that the connection between the background pycnocline depth and the depth of mid-latitude heat penetration under forcing is not a happenstance of ocean geometry. Instead, it emerges because the mid-latitudes dominate pycnocline ventilation (Khatiwala et al., 2012; Sallée et al., 2010; Newsom et al., 2020; Morrison et al., 2022). Thus the pycnocline depth should largely reflect how deeply these water masses penetrate the interior in the mean state, signifying the ocean volume available to sequester heat sourced in these regions under climate forcing.

This argument is supported by the relationship between Southern Ocean ventilation and both pycnocline depth (Gnanadesikan, 1999; Kong & Jansen, 2022; Nikurashin & Vallis, 2011, 2012) and OHUE (Marshall & Zanna, 2014; Saenko et al., 2018) implied by theory and found in Green's Function experiments (Newsom et al., 2020). It is also supported by the relationship between the vertical density gradient in the Southern Ocean (Bourgeois et al., 2022; Liu et al., 2023; Terhaar et al., 2021) and the efficiency of regional and global heat and carbon uptake. Further support comes from recent work (Newsom et al., 2022) demonstrating a strong correlation between the global pattern of pycnocline depth (defined as the e-folding depth of the vertical density profile) and of passive heat storage under radiative forcing. A similar relationship was noted for passive heat and carbon sequestration patterns (Bronselaer & Zanna, 2020). Together, these studies imply that the same processes that establish the depth of the pycnocline—in large part, ventilation from the Southern Ocean and mid-latitudes—are key controls on the sequestration of heat and other tracers in the interior ocean.

In what follows, we show that in both CMIP5-6 and the MITgcm: (a) there is a strong relationship between OHUE and the depth and stratification of the pycnocline depth; and (b) this relationship emerges because of the dominant
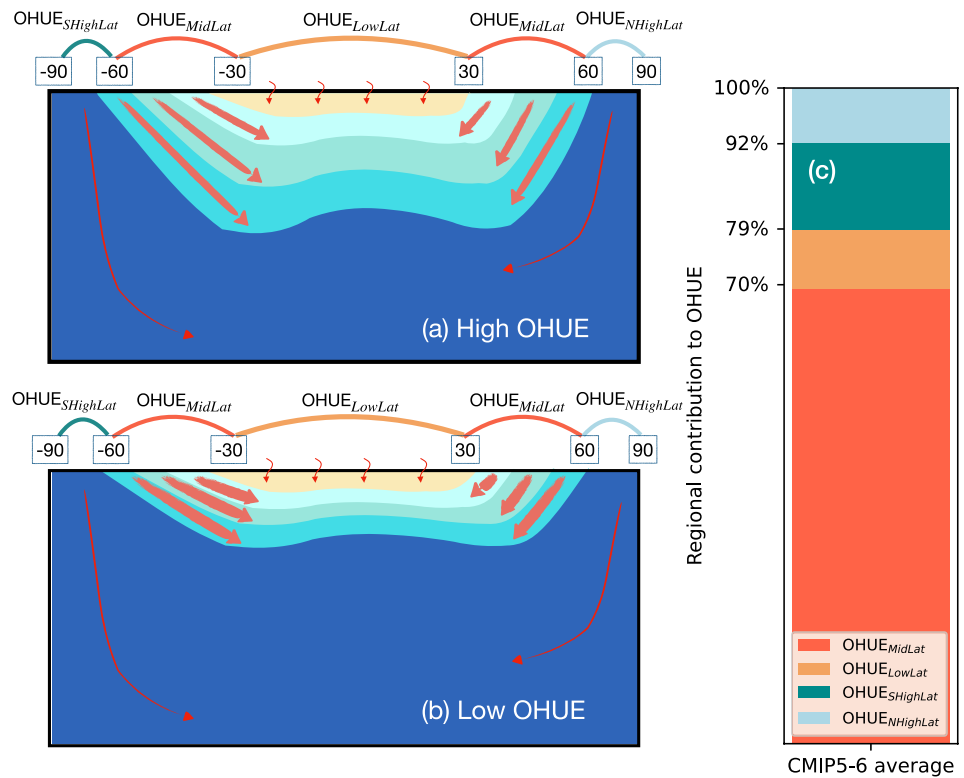
Figure 1. (Left column) schematic of the relationship of Ocean Heat Uptake Efficiency (OHUE) and pycnocline depth, contrasting a high OHUE state (a) and a low OHUE state (b). These panels illustrate that a deeper pycnocline layer will be associated with weaker stratification within, and steeper outcropping slopes of, pycnocline water masses. All heat uptake that occurs along outcropping mid-latitude isopycnals will thus penetrate deeper into the interior for the deep pycnocline state (compare large red arrows between panels (a) and (b)) and more efficiently mitigate global surface warming. Here we depict the same net heat uptake (reflected by the size of the arrows), such that (a)–(b) differ only in the depth of heat penetration. Panels a–b also schematize the different regional components of global OHUE and their meridional extent (as described in Section 2), while panel (c) shows the relative contribution of each regional component to global OHUE (or, OHUE), as discussed in Section 3. Note the size of the red arrows on a-b signifies the regional fraction of global ocean heat uptake.

role of mid-latitudes in setting OHUE. We will argue that differences in pycnocline depth (and, by implication, mid-latitude ventilation) across models also helps to explain inter-model spread in OHUE. We test these ideas by decomposing global OHUE into four regional components, namely the mid-latitudes, tropical and subtropical latitudes, northern high latitudes, and southern high latitudes, as depicted on Figure 1. This regional decomposition is used to quantify each region's relationship to global OHUE and pycnocline depth. The models and metrics used are described in Section 2 and our results are presented in Section 3. We discuss and summarize our findings in Section 4.

2. Methods

2.1. Model Ensembles

We primarily explore the link between OHUE and stratification in 28 CMIP5-6 AOGCMs (listed in Figure 2a), subjected to a historical and then an RCP 8.5 (CMIP5) or SSP585 (CMIP6) future forcing scenario. Anomalies in all CMIP variables are defined as the average value of each over years 2090–2100 minus its average during 1850–1890. Note that the regression coefficients between various metrics and OHUE components (defined below) are not significantly different between CMIP5 and CMIP6 (at the 5% level), thus we combine the ensembles unless otherwise noted.

The MITgcm ensemble, described in depth by Huber and Zanna (2017); Zanna, Brankart, et al. (2019), is complementary to CMIP5-6. MITgcm ensemble members differ in their mesoscale eddy diffusivity (κ_{GM}, in the range 0–1,600 m^{2}s^{-1}), vertical diffusivity (κ_ν, in the range 0.1–1.0 cm^2 s^{-1} in the top $\approx$2,500 m, increasing to 1.1–2.0 cm^{2}s^{-1} in the bottom $\approx$2,500 m) or surface salinity, temperature, and air-sea flux pattern (F), which are based on CMIP5. After a 1000 years spin-up, all experiments are driven by surface salinity, temperature, and air-sea fluxes from the 1%CO$_2$ CMIP5 experiment, either in the multi-model mean (for κ_{GM} and κ_ν perturbations), or from
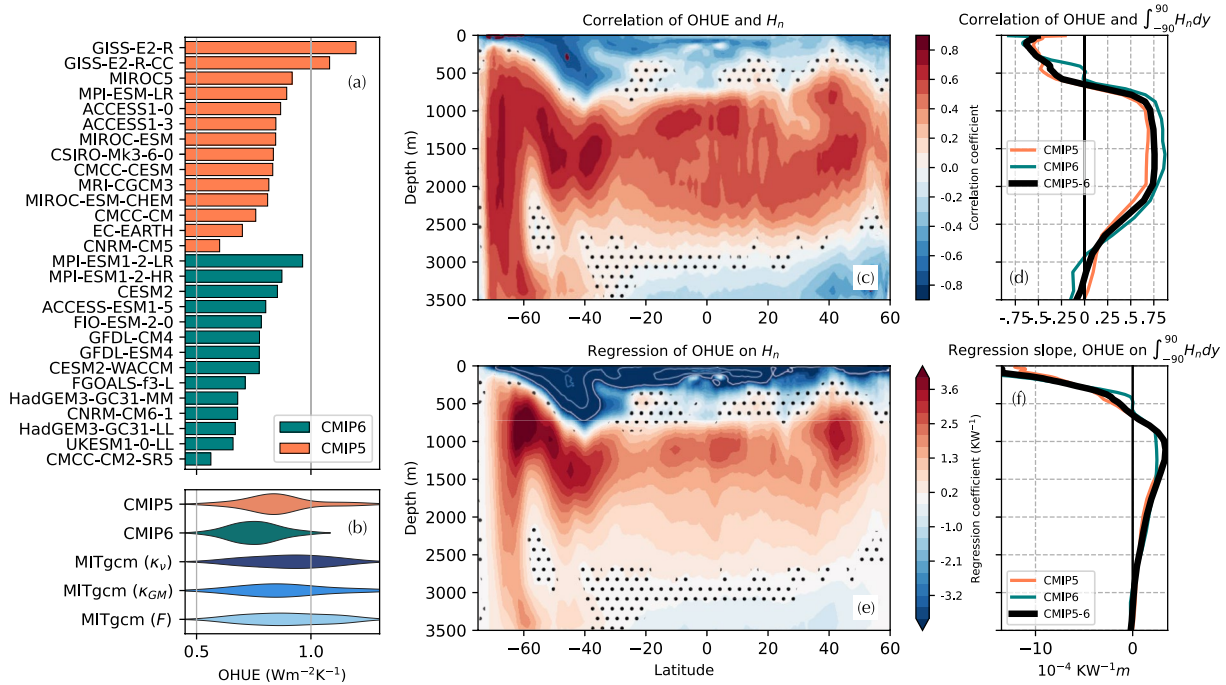
Figure 2. (a) Ocean Heat Uptake Efficiency (OHUE) (Equation 1) for CMIP5 models (orange) and CMIP6 models (teal). (b) The distribution of OHUE in CMIP5, CMIP6 and in the MITgcm experiments. (c) Correlation of OHUE and normalized global heat storage and $H_n(y, z)$ (see text). (d) Same as (c), but for the meridional sum of H_n at each depth. (e) The regression coefficient of OHUE on $H_n(y, z)$. (f) Same as (e), but for the meridional sum of H_n. Panels (e)–(f) illustrate that a key inter-model difference is the increased redistribution of anomalous heat from the upper ocean ($<\approx 600$ m) into the intermediate ocean (≈ 600–$1,500$ m) in high OHUE models, as compared to low OHUE models. Note that stippling in this and the following figures shows where significance is below the 95th percentile.

individual models (for F perturbations). Note that the ranges in κ_ν and κ_{GM} are not meant to span observational uncertainty, but to drive a wide spread in pycnocline depth—in reality, observed upper ocean κ_ν is closer to 0.1 cm^{2}s^{-1} (Ledwell et al., 1993) and mesoscale eddy fluxes, though less constrained, are non-zero. Note however the κ_{GM} range is based on CMIP5 values (see Downes and Hogg (2013) and Huber and Zanna (2017)). All anomalies are calculated at the time of CO_2 doubling. Ranges of OHUE for each set of experiments are shown in Figure 2b.

In sum, CMIP5-6 is a state-of-the-art ensemble of opportunity that samples both structural and parameter uncertainty, while the more idealized MITgcm ensemble systematically perturbs processes known to alter stratification, (Gnanadesikan, 1999; Nikurashin & Vallis, 2011) in order to test our hypothesis across a wide range of parameter space. In doing so, this latter ensemble tests conflicting theories of OHUE controls (i.e., κ_{GM} and Southern Ocean surface salinity) by varying these processes individually.

2.2. OHUE Definitions

Traditionally, OHUE is defined as a global average quantity, for example, Equation 1. Here, we introduce a complementary definition of a "regional" OHUE. This allows us to partition the global OHUE into several regional components, each OHUE$_R$:

$$\text{OHUE}_R \equiv \frac{\int_{A_R} \text{N}(x, y) dA}{A_G \text{SST}}. \tag{2}$$

Here, A_R is the surface area of a given region, $A_G = \sum_R A_R$ is the global surface area, N(x, y) is the local anomaly in surface heat flux at each latitude and longitude, SST is the global mean sea-surface temperature anomaly, and the units of OHUE$_R$ are Wm^{-2} K^{-1}. In this study, we focus on four regional components associated with different mechanisms of heat uptake, $\text{OHUE}_R = (\text{OHUE}_{MidLat}, \text{OHUE}_{LowLat}, \text{OHUE}_{SHighLat}, \text{OHUE}_{NHighLat})$:

1. OHUE$_{MidLat}$: the mid-latitude OHUE calculated with Equation 2 using the area between 30 and 60° in both hemispheres;
2. OHUE$_{LowLat}$: the subtropical and tropical OHUE, calculated between 30°N/S;

3. OHUE$_{SHighLat}$: the Southern high-latitude OHUE, calculated south of 60°; and
4. OHUE$_{NHighLat}$: the Northern high-latitude OHUE, calculated north of 60°N.

Together,

$$\text{OHUE} = \text{OHUE}_{MidLat} + \text{OHUE}_{LowLat} + \text{OHUE}_{SHighLat} + \text{OHUE}_{NHighLat}, \tag{3}$$

where OHUE is the global OHUE, defined in Equation 1 and equivalently in Equation 2... using global ocean area, A_G.

2.3. Stratification Metrics

Our hypothesis centers around global stratification. To illustrate the interior stratification pattern, we use the zonal-mean (denoted by an overbar) Brunt–Väisälä frequency, $\overline{N^2}(y, z) = g/\rho_0 \partial\rho/\partial z$, assuming $\partial\rho/\partial z > 0$, calculated from $\rho(x, y, z)$ and then zonally averaged. Here ρ is the potential density referenced to 2000 dbar, which we use to avoid biasing our density coordinate to the surface or abyssal ocean, especially important for Southern Ocean and intermediate water masses (e.g., Newsom & Thompson, 2018; Waugh et al., 2019). However, all results are robust to the choice of reference pressure.

We characterize this stratification pattern through a representative scalar metric—the pycnocline depth. While the pycnocline is often identified as the bottom of the shallow subtropical gyres and mode waters (e.g., Feucher et al. (2019)), our goal is to instead identify the depth to which mid-latitude sourced water masses penetrate. This depth is also co-located with a significant change in the vertical stratification (see Figure S2 in Supporting Information S1), which we approximate in practice as the e-folding depth of the vertical density distribution, modified to exclude the strongly stratified surface gyres as follows (also see Text S1 in Supporting Information S1 for expanded discussion). We first take the zonal mean of the density field, $\overline{\rho}(y, z)$. We then mask out all density classes in $\overline{\rho}$ less than $\overline{\rho}_{gyre}$, where $\overline{\rho}_{gyre}$ is the zonal-mean density below the base of the winter mixed layer, and thus are ventilated, at 45°S that is, $\overline{\rho}_{gyre} \equiv \overline{\rho}(45S, 350m)$. This depth (350m) approximates the average observed winter mixed layer depth, which in reality varies hundreds of meters with latitude (Buongiorno Nardelli et al., 2017), though note that our results are insensitive to this choice below ≈100 m (see Text S1 and Figure S1 in Supporting Information S1). We chose 45°S because it is an extreme in the model- and zonal-mean meridional density gradient, which should be associated with edge of the gyre.

This leaves the "interior density field," $\overline{\rho^*}(y, z)$, where y is latitude, z depth, and the superscript "*" signifies all density classes greater than isopycnal $\overline{\rho}_{gyre}$, isolating the density profile of the waters predominantly sourced in the mid- and high latitudes. Since density increases downwards, $\overline{\rho^*}(y, B) - \overline{\rho^*}(y, z) > 0$, where $z = B(y)$ at the bottom of the ocean. Hence we derive a normalized vertical density coordinate $\overline{\rho}_{norm}$ which ranges from zero at the ocean bottom to unity at the shallowest depth considered:

$$\overline{\rho}_{norm}(y, z) = \frac{\overline{\rho^*}(y, B) - \overline{\rho^*}(y, z)}{\max_z\left(\overline{\rho^*}(y, B) - \overline{\rho^*}(y, z)\right)}, \tag{4}$$

where "$\max_z X(y, z)$" means the largest value of X for given latitude y. The largest value of $\overline{\rho^*}(y, B) - \overline{\rho^*}(y, z)$ in the denominator in Equation 4 belongs to the shallowest z considered, either the surface or the depth of ρ_{gyre}. Thus $\overline{\rho}_{norm}$ ranges from zero to one from its deepest to shallowest z, capturing the shape of vertical variation in zonal-mean density below the shallow surface gyres across models (see Figure S2 in Supporting Information S1). We define the pycnocline depth, d, as the depth at which $\overline{\rho}_{norm} = 1/e$ at each latitude, which assumes $\overline{\rho}_{norm}$ can be approximated as an exponential profile, such that $\overline{\rho}_{norm} = e^{-z/d}$. In what follows, we will refer to the average pycnocline depth between 60°S/N as the "pycnocline depth" unless otherwise noted.

Notably, the relationships discussed in Section 3 are quite robust to other pycnocline definitions (Text S1 and S2 and Figures S3 and S4 in Supporting Information S1); this definition was used instead of, for instance, an isopycnal surface, due to the somewhat arbitrary nature of selecting the appropriate isopycnal in practice. Note also that the pycnocline depth covaries strongly with other measures of mid-latitude ventilation strength, such as the slopes or stratification of Southern Ocean isopycnals (at $R = 0.9$ and $R = 0.95$, respectively), as discussed in Text S3 in Supporting Information S1. This interconnection, between Southern Ocean and global stratification, affirms the dominance of the Southern Ocean in ventilating the global pycnocline, for example, Sallée et al. (2010), Khatiwala et al. (2012), Morrison et al. (2022).

3. Results

3.1. Global Heat Uptake Efficiency

We begin by examining global aspects of OHUE (=N/SST) in CMIP5-6. As noted in Section 1, there is a wide spread in OHUE across CMIP5-6 models. The ratio of the standard deviation in OHUE to its ensemble mean, that is, the spread, is 17% in CMIP5 and 13% in CMIP6 (Figure 2a). Individually, the spreads in surface heat flux anomaly, N, is 15% and 16% in CMIP5 and CMIP6, and 21% and 22% in SST. The spread in OHUE is generally smaller than N or SST individually because N and SST are correlated (not shown), more so in CMIP6, in which the correlation between N and SST is stronger (at $R \approx 0.88$) than in CMIP5 ($R \approx 0.68$). The mean OHUE is also smaller in CMIP6, which may result from the higher climate sensitivity in this ensemble (Zelinka et al., 2020).

Differences in OHUE across CMIP5-6 models are associated with different vertical profiles of warming, quantified by the heat storage per unit depth and latitude, $H(y, z) \equiv \int_0^{360} \theta(x, y, z) dx$ (units K m), where θ is the anomaly in ocean temperature (see Section 2.1). Models also differ in their total heat storage, $\mathcal{H} = \int_B^0 \int_{-90}^{90} H \, dy \, dz$. Therefore, to compare the pattern of heat storage in each model, relative to one another, we consider the normalized heat storage pattern $H_n(y, z) \equiv H(y, z)/\mathcal{H}$, Figures 2c–2f illustrates the correlation of OHUE and H_n with latitude and depth, the latter for which we sum H_n meridionally. Figures 2c and 2d shows that greater OHUE is associated with relatively more heat storage below $\approx$600m, and less heat storage above $\approx$600 m (Figure 2d), particularly within the Southern mid-latitudes, $\approx$55–30°S, see Figure 2c. This pattern implies a larger net global heat flux across $\approx$600 m in models with higher OHUE, consistent with Saenko et al. (2018) and Kostov et al. (2014).

Critically, while the correlation of OHUE and H_n is positive between $\approx$600 and 3000 m depth (Figure 2d), the majority (>80%) of anomalous heat is stored in the upper 2,000 m in all models. Thus, inter-model differences in vertical heat storage patterns, and the correlation of these patterns to OHUE, are most impactful in the upper 2000 m, that is, they involve larger quantities of heat. To illustrate this, we also show the regression coefficient for OHUE on H_n at each latitude (Figure 2e) and depth (Figure 2f). This regression pattern also crosses zero at $\approx$600 m, but peaks at $\approx$1200 m—this slope will be larger, for a given correlation strength, where the mean heat content across models is greater. Regression patterns illustrate that higher OHUE is primarily associated with processes moving heat from the surface ocean (<600 m depth) into intermediate depths ($\approx$600–2,000 m).

We hypothesize that greater OHUE, and thus greater heat storage across intermediate depths, is linked to a deeper global pycnocline and, correspondingly, weaker pycnocline stratification in the background state. To test this hypothesis, we examine the relationship between OHUE and the zonal-mean stratification, $\overline{N^2}$ (defined in Section 2.3 and shown in Figure 3a in the ensemble mean) in CMIP5-6. Figure 3b shows the correlation of these quantities as a function of latitude and depth.

A general pattern emerges in Figure 3b, in which greater OHUE is correlated with a weaker stratification of the water masses that outcrop at the mid-latitude surface (latitudes $\approx$60°–30° in both hemispheres, see isopycnals in Figure 3a) and fill the basin interior above $\approx$1300 m. The weakly stratified water is largely bounded below by the pycnocline depth (defined in Section 2.3). The CMIP5-6 mean pycnocline depth is indicated as a function of latitude by the thick black line in Figure 3a, and for individual AOGCMs by the lines in Figure 3b, which are colored by OHUE strength, and show that the pycnocline is deeper in models with greater OHUE.

The relationship between OHUE and pycnocline depth is quantified by the correlation of $R = 0.83$ across CMIP5-6 AOGCMs between OHUE and the average 60°S–60°N pycnocline depth (Figure 3c). There is a larger spread in pycnocline depth in CMIP5 than CMIP6, corresponding to a larger OHUE spread, potentially linked to differences in tidal mixing parameterizations, among others factors, between ensembles (Saenko & Merryfield, 2005). Across the MITgcm ensemble, the pycnocline-OHUE relationship is even stronger, at $R = 0.92$ (Figure 3d). Together, these clear and consistent relationships support our hypothesis that OHUE is closely related to the stratification of the global pycnocline.

3.2. Regional Heat Uptake Efficiency

3.2.1. Mid-Latitudes

Our regional OHUE decomposition (Equation 3) clarifies the importance of the mid-latitude regions in setting the global relationships between OHUE and stratification discussed in Section 3.1. Component OHUE$_{MidLat}$
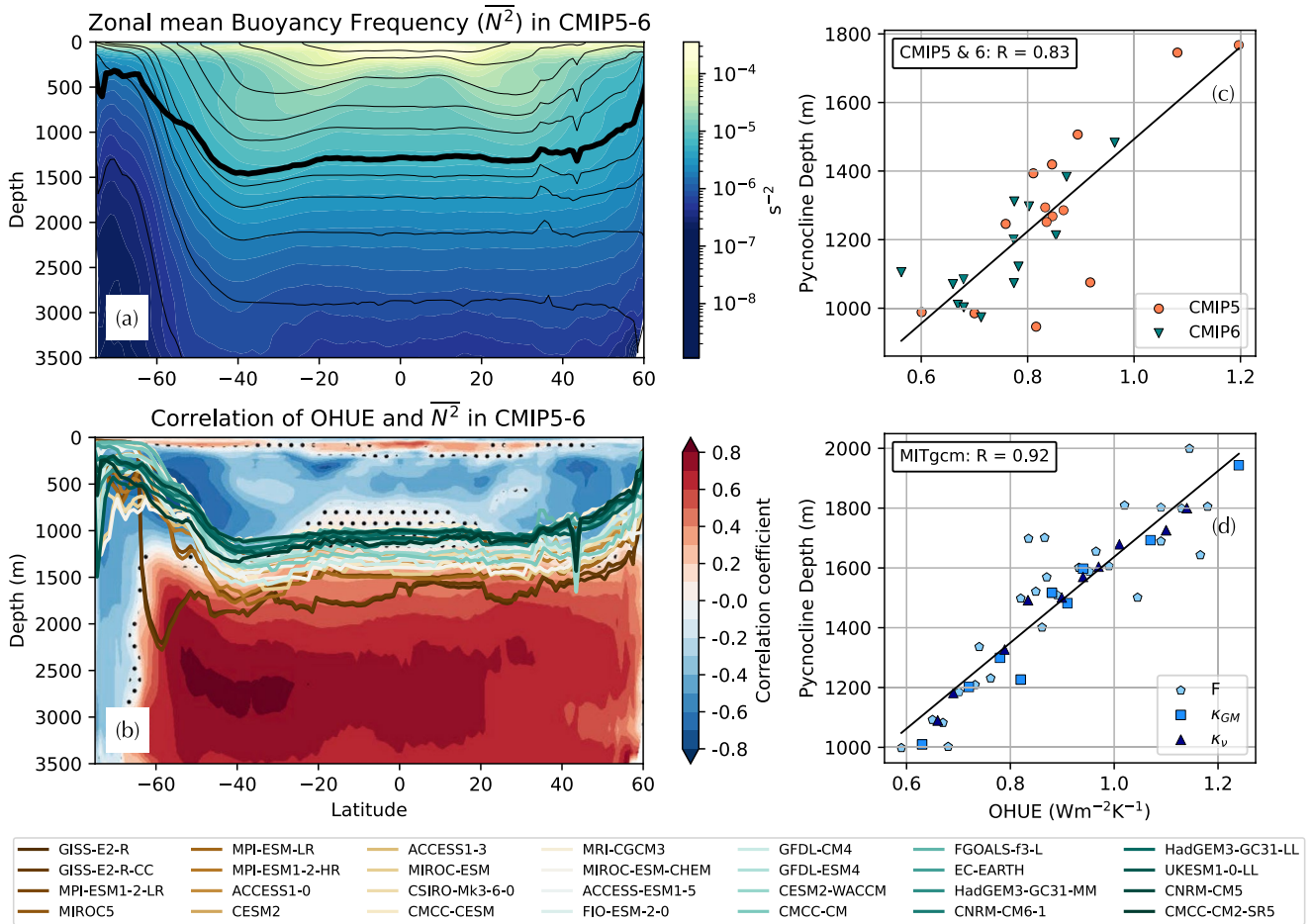
Figure 3. (a) The CMIP5-6 ensemble mean zonal-mean buoyancy frequency $\left(\overline{N^2}\right)$ is shown to illustrate the mean stratification distribution with depth and latitude. Overlaid on (a) is the ensemble mean pycnocline depth (thick black) and several isopycnals (spaced by $\approx$0.5 kg/m^3 above the pycnocline and $\approx$0.1 kg/m^3 below it) to show where waters above $\approx$1,500 m outcrop. (b) Point-wise correlation between $\overline{N^2}$ and Ocean Heat Uptake Efficiency (OHUE) in CMIP5-6 (b). Overlaid on (b) is pycnocline depth, defined via Equation 4, and colored from high to low OHUE across models (brown to green colors). (c)-(d) OHUE versus the average pycnocline depth in CMIP5-6 (c) and the MITgcm (d). Note that on (b), the stippling shows where the correlation is not significant to the 95th percentile. Also note that $\overline{N^2}$ is 2–3 orders of magnitude smaller below $\approx$1,500 m than above it, so while these deeper correlations are significant, they involve small vertical density differences. This distinction is evident in the regression of OHUE on $\overline{N^2}$ (Figure S7 in Supporting Information S1).

encapsulates the efficiency of heat uptake, relative to global mean SST, from the region between 30 and 60° in both hemispheres. This region accounts for 70% of the total global anomaly in ocean heat uptake (Figure 1b) in CMIP5-6 during the period considered (2090–2100), as well as around 70% of the inter-model variance in OHUE, in both CMIP5 and CMIP6 (Fig. S6). This is consistent with the historical dominance of observed heat uptake from these regions (e.g., Frölicher et al., 2015; Zanna, Khatiwala, et al., 2019; Cheng et al., 2022).

To probe the relationship of OHUE$_{MidLat}$ and $\overline{N^2}$, we calculate their correlation at each latitude and depth (Figure 4a). As for (global) OHUE (Figure 3b), a clear fingerprint emerges, linking greater OHUE$_{MidLat}$ to more weakly stratified water-masses above the pycnocline, both within the Southern Ocean and in the basins to its north. While the relationship of OHUE$_{MidLat}$ to the stratification is qualitatively similar to that of OHUE (Figure 3b), it is stronger both within the Southern Ocean, where local stratification and OHUE$_{MidLat}$ are correlated at $R \geq 0.75$ in CMIP5-6 (Figure S8 in Supporting Information S1), and more coherent into the interior across depths $\approx$500–1500 m (Figure 4a).

The relationship between OHUE$_{MidLat}$ and pycnocline depth is similarly robust, and apparent in Figure 4a. The correlation of average 60°S–60°N pycnocline depth with OHUE$_{MidLat}$ is about as strong as with OHUE in both CMIP5-6 AOGCMs ($R = 0.86$, Figure 4b) and the MITgcm ensemble ($R = 0.87$, Figure 4c). These relationships support the idea that more heat can be absorbed in the mid-latitudes, for a given global surface warming, when regional ventilation is strong, as evidenced by a deeper, less stratified pycnocline in the background state.
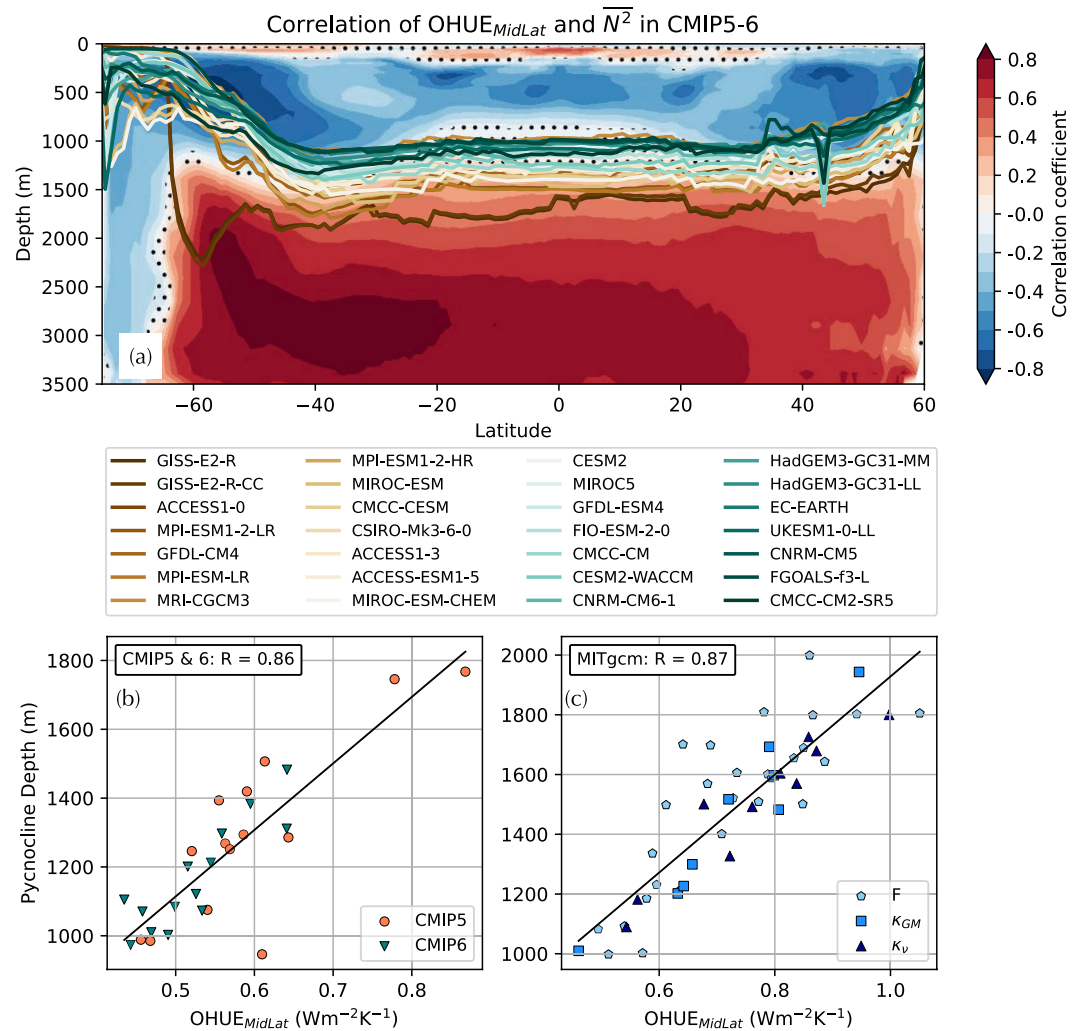
Figure 4. (a) The point-wise correlation between $OHUE_{MidLat}$ and $\overline{N^2}$ in CMIP5-6. Overlaid is the pycnocline depth, which is colored from high to low $OHUE_{MidLat}$. (b) As in Figure 3c, but for the $OHUE_{MidLat}$ in CMIP5-6. (c) As in Figure 3d, but for the $OHUE_{MidLat}$ in MITgcm.

3.2.2. The Low and High Latitudes

OHUE is also substantially influenced by processes outside of the mid-latitudes. The remaining ≈30% of OHUE in CMIP5-6 (as regionally partitioned in Section 2) is accounted for by the southern high latitudes ($OHUE_{SHighLat} \approx 13\%$), the northern high latitudes ($OHUE_{NHighLat} \approx 9\%$) and the low-latitudes ($OHUE_{LowLat} \approx 10\%$) (Figure S6 in Supporting Information S1) on average. To understand how these regions influence the relationship of OHUE and the pycnocline depth, we examine the point-wise correlation between $\overline{N^2}$ and each of these regional OHUE components (Figure S9 in Supporting Information S1). Unlike OHUE and $OHUE_{MidLat}$, no clear or physically meaningful patterns emerges for any of them, with two exceptions: $OHUE_{SHighLat}$ is higher for models with weak full-depth stratification south of 60S, and $OHUE_{NHighLat}$ is somewhat correlated ($R \leq 0.45$) with stronger stratification between ≈ 1,800 − 3,000 m. Accordingly, we find no clear relationship between these OHUE components and average 60°S–60°N pycnocline depth in CMIP5-6. Essentially, the high and low latitude regions add random scatter to the relationship between OHUE and stratification, which is mediated through mid-latitude processes.

4. Discussion and Conclusions

Our results reveal a strong connection between global OHUE and global stratification, as quantified by the pycnocline depth. We argue that the connection exists because the pycnocline is a proxy for the depth of mid-latitude

ventilation in the background state, and that these same ventilation processes make the largest contribution to global OHUE under anthropogenic forcing. A corollary of these results is that heat uptake efficiency outside the mid-latitudes has little direct connection to subtropical pycnocline depth, perhaps unsurprisingly, as no clear mechanism would predict such a connection.

These findings align with previous work relating both background stratification to Southern Ocean processes (Gnanadesikan, 1999; Kong & Jansen, 2022; Marshall & Zanna, 2014; Nikurashin & Vallis, 2011, 2012), and the depth of heat penetration to the vertical density profile (Marshall & Zanna, 2014). Studies that connect high OHUE to weaker Southern Ocean eddy activity (i.e., lower κ_{GM}, Kuhlbrodt & Gregory, 2012; Saenko et al., 2018) are particularly relevant, since, all else being equal, reducing κ_{GM} will increase Southern Ocean ventilation and pycnocline depth (Figures 3 and 4; Gnanadesikan, 1999; Marshall & Zanna, 2014). Yet, our argument here is that ventilation is also influenced by many other processes, including Southern Ocean wind stress, surface salinity,and temperature, interior mixing and frontal dynamics, and surface buoyancy flux (Morrison et al., 2022; Sallée et al., 2010; Kong & Jansen, 2022), all of which may influence OHUE. Indeed, Southern Ocean surface salinity correlates significantly with both OHUE (Liu et al., 2023) and global anthropogenic carbon uptake in CMIP6 (Terhaar et al., 2021), consistent with the correlation between Southern Ocean vertical stratification and regional heat and carbon uptake efficiency (Bourgeois et al., 2022), and leading Liu et al. (2023) to hypothesize that Southern Ocean salinity is a primary determinant of OHUE.

Our MITgcm results, in which individual parameters—including κ_{GM} and surface salinity—vary widely, show instead that no individual process controls OHUE. Instead, each affects OHUE through mid-latitude ventilation, as measured in the aggregate by pycnocline depth. Consistent with Saenko et al. (2018), our experiments show a strong relationship between κ_{GM} and OHUE, where stronger parameterized eddies lead to lower OHUE, a more stratified ocean and a shallower pycnocline (pycnocline depth and OHUE correlate at $R = 0.98$ in the κ_{GM} ensemble). Yet, we also show an inverse, and equally strong, relationship in the κ_{ν} ensemble: greater κ_{ν} increases OHUE, stratification, and pycnocline depth (which also correlates with OHUE at $R = 0.98$). The less straightforward range of OHUE in the air-sea flux experiments (F) is equally wide and correlated to stratification, evidencing of the strong sensitivity in the MITgcm to high-latitude, and north-south gradients of, surface forcing (Kostov et al., 2019). Note that, while the MITgcm correlations are strong, this model resolution is coarse and the parameterizations relatively simple (Huber & Zanna, 2017). This enabled a large ensemble and simple physical interpretations.

The correlation of pycnocline depth and OHUE (Figure 3c) also implies that the spread in pycnocline depth in CMIP5-6 explains around 69% of the spread in OHUE (calculated here as R^2), and 74% of the spread in OHUE$_{MidLat}$. This is supported by a key difference between high and low OHUE CMIP5-6 models—high OHUE models store relatively less heat in the upper ≈ 600 m and more across intermediate depths (600–1,500 m, Figure 2), consistent with Kostov et al. (2014), Saenko et al. (2018), and Liu et al. (2023). These depths are collocated with the clearest and most predictive differences in stratification between high and low OHUE models (see the strong negative correlations above ≈ 1500m in Figures 3b and 4a), implying that the capacity to sequester heat here is linked to the weak stratification signature originating at the mid-latitude surface. Importantly, our MITgcm experiments highlight that better eddy closures in coarse resolution models (e.g., Jansen et al., 2019; Zanna & Bolton, 2020) would help to reduce this persistent spread in both global stratification and OHUE.

The ocean physics we discuss in the context of OHUE may additionally modulate future climate through a surface warming "pattern effect" (Armour et al., 2013; Gregory & Andrews, 2016; Stevens et al., 2016; Xie, 2020). Recent work highlights how surface warming patterns are disproportionately influenced by heat uptake and warming in the Southern Ocean (Dong et al., 2022; Lin et al., 2021), a region with a strong influence on climate sensitivity (Andrews et al., 2015; Zelinka et al., 2020). However, the link between OHUE and the pattern effect is thus far unclear. Given the central role of the Southern Ocean and mid-latitudes in our study, a key goal of future work will be to develop a more unified understanding of how these regions influence transient climate change, incorporating their inter-dependent effects.

To that end, this work offers the hope of constraining future OHUE and warming patterns through contemporary oceanic observations, for instance, of pycnocline depth or stratification. In turn, this may reduce uncertainty in global sea level projections, surface warming, and the ocean's long-term capacity store anthropogenic carbon (e.g., Bronselaer and Zanna (2020); Terhaar et al. (2021); Bourgeois et al. (2022)).

Data Availability Statement

The CMIP6 and CMIP5 data are available through the Earth System Grid Federation system (ESGF; https://esgf-node.llnl.gov/search/cmip6/, https://esgf-node.llnl.gov/search/cmip5/, respectively), and the models and ensemble members used in this study are listed in Table S1 and S2 in Supporting Information S1 and in Figure 1. The figure-making code uses Matplotlib version 3.5.2 (Caswell et al., 2022) and is publicly available in the Zenodo repository (Newsom, 2023).

References

Andrews, T., Gregory, J. M., & Webb, M. J. (2015). The dependence of radiative forcing and feedback on evolving patterns of surface temperature change in climate models. *Journal of Climate*, *28*(4), 1630–1648. https://doi.org/10.1175/JCLI-D-14-00545.1

Armour, K. C., Bitz, C. M., & Roe, G. H. (2013). Time-varying climate sensitivity from regional feedbacks. *Journal of Climate*, *26*(13), 4518–4534. https://doi.org/10.1175/JCLI-D-12-00544.1

Armour, K. C., Marshall, J., Scott, J. R., Donohoe, A., & Newsom, E. R. (2016). Southern Ocean warming delayed by circumpolar upwelling and equatorward transport. *Nature Geoscience*, *9*(7), 549–554. https://doi.org/10.1038/ngeo2731

Bourgeois, T., Goris, N., Schwinger, J., & Tjiputra, J. F. (2022). Stratification constrains future heat and carbon uptake in the Southern Ocean between 30°S and 55°S. *Nature Communications*, *13*(1), 1–8. https://doi.org/10.1038/s41467-022-27979-5

Bronselaer, B., & Zanna, L. (2020). Heat and carbon coupling reveals ocean warming due to circulation changes. *Nature*, *584*(7820), 227–233. https://doi.org/10.1038/s41586-020-2573-5

Buongiorno Nardelli, B., Guinehut, S., Verbrugge, N., Cotroneo, Y., Zambianchi, E., & Iudicone, D. (2017). Southern ocean mixed-layer seasonal and interannual variations from combined satellite and in situ data. *Journal of Geophysical Research: Oceans*, *122*(12), 10042–10060. https://doi.org/10.1002/2017JC013314

Caswell, T. A., Droettboom, M., Lee, A., de Andrade, E. S., Hoffmann, T., Klymak, J., et al. (2022). matplotlib/matplotlib: Rel: v3.5.2 [Software]. Zenodo. https://doi.org/10.5281/zenodo.6513224

Cheng, L., Schuckmann, K. v., Abraham, J., Trenberth, K., Mann, M., Zanna, L., et al. (2022). Past and future ocean warming. *Nature Review*, 1–39. https://doi.org/10.1038/s43017-022-00345-1

Cheng, L., Trenberth, K. E., Fasullo, J., Boyer, T., Abraham, J., & Zhu, J. (2017). Improved estimates of ocean heat content from 1960 to 2015. *Science Advances*, *3*(3), 1–11. https://doi.org/10.1126/sciadv.1601545

Church, J. A., Godfrey, J. S., Jackett, D. R., & McDougall, T. J. (1991). A model of sea level rise caused by ocean thermal expansion. *Journal of Climate*, *4*(4), 438–456. https://doi.org/10.1175/1520-0442(1991)004⟨0438:AMOSLR⟩2.0.CO;2

Couldrey, M. P., Gregory, J. M., Boeira Dias, F., Dobrohotoff, P., Domingues, C. M., Garuba, O., et al. (2021). *What causes the spread of model projections of ocean dynamic sea-level change in response to greenhouse gas forcing? (No. January)*. Springer Berlin Heidelberg. https://doi.org/10.1007/s00382-020-05471-4

Dong, Y., Pauling, A. G., Sadai, S., & Armour, K. C. (2022). Antarctic ice-sheet meltwater reduces transient warming and climate sensitivity through the sea-surface temperature pattern effect. *Geophysical Research Letters*, *49*(24), 1–11. https://doi.org/10.1029/2022GL101249

Downes, S. M., & Hogg, A. M. (2013). Southern ocean circulation and eddy compensation in CMIP5 models. *Journal of Climate*, *26*(18), 7198–7220. https://doi.org/10.1175/JCLI-D-12-00504.1

Exarchou, E., Kuhlbrodt, T., Gregory, J. M., & Smith, R. S. (2015). Ocean heat uptake processes: A model intercomparison. *Journal of Climate*, *28*(2), 887–908. https://doi.org/10.1175/JCLI-D-14-00235.1

Feucher, C., Maze, G., & Mercier, H. (2019). Subtropical mode water and permanent pycnocline properties in the world ocean. *Journal of Geophysical Research: Oceans*, *124*(2), 1139–1154. https://doi.org/10.1029/2018JC014526

Frölicher, T. L., Sarmiento, J. L., Paynter, D. J., Dunne, J. P., Krasting, J. P., & Winton, M. (2015). Dominance of the southern ocean in anthropogenic carbon and heat uptake in CMIP5 models. *Journal of Climate*, *28*(2), 862–886. https://doi.org/10.1175/JCLI-D-14-00117.1

Gent, P. R., & McWilliams, J. C. (1990). Isopycnal mixing in ocean circulation models. *Journal of Physical Oceanography*, *20*(1), 150–155. https://doi.org/10.1175/1520-0485(1990)020⟨0150:imiocm⟩2.0.co;2

Gnanadesikan, A. (1999). A simple predictive model for the structure of the oceanic pycnocline. *Science*, *283*(5410), 2077–2079. https://doi.org/10.1126/science.283.5410.2077

Gregory, J. M., & Andrews, T. (2016). Variation in climate sensitivity and feedback parameters during the historical period. *Geophysical Research Letters*, *43*(8), 3911–3920. https://doi.org/10.1002/2016GL068406

Gregory, J. M., Bouttes, N., Griffies, S. M., Haak, H., Hurlin, W. J., Jungclaus, J., et al. (2016). Intercomparison project (FAFMIP) contribution to CMIP6: Investigation of. *Geoscientific Model Development*, *9*(11), 3993–4017. https://doi.org/10.5194/gmd-9-3993-2016

Gregory, J. M., & Mitchell, J. F. (1997). The climate response to CO_2 of the Hadley Centre coupled AOGCM with and without flux adjustment. *Geophysical Research Letters*, *24*(15), 1943–1946. https://doi.org/10.1029/97GL01930

Huber, M. B., & Zanna, L. (2017). Drivers of uncertainty in simulated ocean circulation and heat uptake. *Geophysical Research Letters*, *44*(3), 1402–1413. https://doi.org/10.1002/2016GL071587

Jackett, D. R., & McDougall, T. J. (1997). A Neutral density variable for the World's Oceans. *Journal of Physical Oceanography*, *27*(2), 237–263. https://doi.org/10.1175/1520-0485(1997)027⟨0237:ANDVFT⟩2.0.CO;2

Jansen, M. F., Adcroft, A., Khani, S., & Kong, H. (2019). Toward an energetically consistent, resolution aware parameterization of ocean mesoscale eddies. *Journal of Advances in Modeling Earth Systems*, *11*(8), 2844–2860. https://doi.org/10.1029/2019MS001750

Khatiwala, S., Primeau, F., & Holzer, M. (2012). Ventilation of the deep ocean constrained with tracer observations and implications for radiocarbon estimates of ideal mean age. *Earth and Planetary Science Letters*, *325–326*, 116–125. https://doi.org/10.1016/j.epsl.2012.01.038

Kong, H., & Jansen, M. F. (2022). Time-dependent response of the overturning circulation and pycnocline depth to southern ocean surface wind stress changes. *Journal of Physical Oceanography*, *52*(4), 759–774. https://doi.org/10.1175/JPO-D-21-0214.1

Kostov, Y., Armour, K. C., & Marshall, J. (2014). Impact of the atlantic meridional overturning circulation on ocean heat storage and transient climate change. *Geophysical Research Letters*, *41*(6), 2108–2116. https://doi.org/10.1002/2013gl058998

Kostov, Y., Johnson, H. L., & Marshall, D. P. (2019). AMOC sensitivity to surface buoyancy fluxes: The role of air-sea feedback mechanisms. *Climate Dynamics*, *53*(7–8), 4521–4537. https://doi.org/10.1007/s00382-019-04802-4

Kuhlbrodt, T., & Gregory, J. M. (2012). Ocean heat uptake and its consequences for the magnitude of sea level rise and climate change. *Geophysical Research Letters*, *39*(17), 1–6. https://doi.org/10.1029/2012GL052952

Ledwell, J. R., Watson, A. J., & Law, C. S. (1993). Evidence for slow mixing across the pycnocline from an open-ocean tracer-release experiment. *Nature*, *364*(6439), 701–703. https://doi.org/10.1038/364701a0

Lin, Y. J., Hwang, Y. T., Lu, J., Liu, F., & Rose, B. E. (2021). The dominant contribution of southern ocean heat uptake to time-evolving radiative feedback in CESM. *Geophysical Research Letters*, *48*(9), 1–11. https://doi.org/10.1029/2021GL093302

Liu, M., Soden, B. J., Vecchi, G. A., & Wang, C. (2023). The spread of ocean heat uptake efficiency traced to ocean salinity. *Geophysical Research Letters*, *50*(4), 1–10. https://doi.org/10.1029/2022GL100171

Lyu, K., Zhang, X., Church, J. A., & Wu, Q. (2020). Processes responsible for the southern hemisphere ocean heat uptake and redistribution under anthropogenic warming. *Journal of Climate*, *33*(9), 3787–3807. https://doi.org/10.1175/jcli-d-19-0478.1

Marshall, D. P., & Zanna, L. (2014). A conceptual model of ocean heat uptake under climate change. *Journal of Climate*, *27*(22), 8444–8465. https://doi.org/10.1175/JCLI-D-13-00344.1

Meyssignac, B., Boyer, T., Zhao, Z., Hakuba, M. Z., Landerer, F. W., Stammer, D., et al. (2019). Measuring global ocean heat content to estimate the Earth energy imbalance. *Frontiers in Marine Science*, *6*, 1–31. https://doi.org/10.3389/fmars.2019.00432

Morrison, A. K., Waugh, D. W., Hogg, A. M. C., Jones, D. C., & Abernathey, R. P. (2022). Ventilation of the southern ocean pycnocline. *Annual Review of Marine Science*, *14*(1), 405–430. https://doi.org/10.1146/annurev-marine-010419-011012

Newsom, E. R. (2023). emilyrosenewsom/OHUE-Pycnocline-relationship: Publication release [Software]. Zenodo. https://doi.org/10.5281/zenodo.8357059

Newsom, E. R., & Thompson, A. F. (2018). Reassessing the role of the indo-Pacific in the Ocean's global overturning circulation. *Geophysical Research Letters*, *45*(12), 422–431. https://doi.org/10.1029/2018GL080350

Newsom, E. R., Zanna, L., & Khatiwala, S. (2022). Relating patterns of added and redistributed ocean warming. *Journal of Climate*, *35*(14), 4627–4643. https://doi.org/10.1175/JCLI-D-21-0827.1

Newsom, E. R., Zanna, L., Khatiwala, S., & Gregory, J. M. (2020). The influence of warming patterns on passive ocean heat uptake. *Geophysical Research Letters*, *47*(18), e2020GL088429. https://doi.org/10.1029/2020GL088429

Nikurashin, M., & Vallis, G. (2011). A theory of deep stratification and overturning circulation in the ocean. *Journal of Physical Oceanography*, *41*(3), 485–502. https://doi.org/10.1175/2010JPO4529.1

Nikurashin, M., & Vallis, G. (2012). A theory of the interhemispheric meridional overturning circulation and associated stratification. *Journal of Physical Oceanography*, *42*(10), 1652–1667. https://doi.org/10.1175/JPO-D-11-0189.1

Raper, S., Gregory, J. M., & Stouffer, R. J. (2002). The role of climate sensitivity and ocean heat uptake on AOGCM transient temperature response. *Journal of Climate*, *15*(1), 124–130. https://doi.org/10.1175/1520-0442(2002)015<0124:trocsa>2.0.co;2

Romanou, A., Marshall, J., Kelley, M., & Scott, J. (2017). Role of the ocean's AMOC in setting the uptake efficiency of transient tracers. *Geophysical Research Letters*, *44*(11), 5590–5598. https://doi.org/10.1002/2017GL072972

Saenko, O. A., Gregory, J. M., Griffies, S. M., Couldrey, M. P., & Dias, F. B. (2021). Contribution of ocean physics and dynamics at different scales to heat uptake in low-resolution aogcms. *Journal of Climate*, *34*(6), 2017–2035. https://doi.org/10.1175/JCLI-D-20-0652.1

Saenko, O. A., & Merryfield, W. J. (2005). On the effect of topographically enhanced mixing on the global ocean circulation. *Journal of Physical Oceanography*, *35*(5), 826–834. https://doi.org/10.1175/JPO2722.1

Saenko, O. A., Yang, D., & Gregory, J. M. (2018). Impact of mesoscale eddy transfer on heat uptake in an eddy-parameterizing ocean model. *Journal of Climate*, *31*(20), 8589–8606. https://doi.org/10.1175/JCLI-D-18-0186.1

Sallée, J. B., Speer, K., Rintoul, S., & Wijffels, S. (2010). Southern ocean thermocline ventilation. *Journal of Physical Oceanography*, *40*(3), 509–529. https://doi.org/10.1175/2009JPO4291.1

Shi, J. R., Xie, S. P., & Talley, L. D. (2018). Evolving relative importance of the Southern Ocean and North Atlantic in anthropogenic ocean heat uptake. *Journal of Climate*, *31*(18), 7459–7479. https://doi.org/10.1175/JCLI-D-18-0170.1

Stevens, B., Sherwood, S. C., Bony, S., & Webb, M. J. (2016). Prospects for narrowing bounds on Earth's equilibrium climate sensitivity. *Earth's Future*, *4*(11), 512–522. https://doi.org/10.1002/2016EF000376

Terhaar, J., Frölicher, T. L., & Joos, F. (2021). Southern Ocean anthropogenic carbon sink constrained by sea surface salinity. *Science Advances*, *7*(18), 1–11. https://doi.org/10.1126/sciadv.abd5964

Todd, A., Zanna, L., Couldrey, M., Gregory, J., Wu, Q., Church, J. A., et al. (2020). Ocean-only FAFMIP: Understanding regional patterns of Ocean heat content and dynamic sea level change. *Journal of Advances in Modeling Earth Systems*, *12*(8), 1–26. https://doi.org/10.1029/2019MS002027

Waugh, D. W., Hogg, A. M., Spence, P., England, M. H., & Haine, T. W. (2019). Response of southern ocean ventilation to changes in midlatitude westerly winds. *Journal of Climate*, *32*(17), 5345–5361. https://doi.org/10.1175/JCLI-D-19-0039.1

Winton, M., Anderson, W. G., Delworth, T. L., Griffies, S. M., Hurlin, W. J., & Rosati, A. J. (2014). Has coarse ocean resolution biased simulations of transient climate sensitivity? *Geophysical Research Letters*, *41*(23), 8522–8529. https://doi.org/10.1002/2014GL061523.Received

Winton, M., Griffies, S. M., Samuels, B. L., Sarmiento, J. L., & Frölicher, T. L. (2013). Connecting changing ocean circulation with changing climate. *Journal of Climate*, *26*(7), 2268–2278. https://doi.org/10.1175/JCLI-D-12-00296.1

Xie, S. (2020). Ocean warming pattern effect on global and regional climate change. *AGU Advances*, *1*(1). https://doi.org/10.1029/2019av000130

Zanna, L., & Bolton, T. (2020). Data-driven equation discovery of ocean mesoscale closures. *Geophysical Research Letters*, *47*(17), 1–13. https://doi.org/10.1029/2020GL088376

Zanna, L., Brankart, J. M., Huber, M., Leroux, S., Penduff, T., & Williams, P. D. (2019). Uncertainty and scale interactions in ocean ensembles: From seasonal forecasts to multidecadal climate predictions. *Quarterly Journal of the Royal Meteorological Society*, *145*(S1), 160–175. https://doi.org/10.1002/qj.3397

Zanna, L., Khatiwala, S., Gregory, J. M., Ison, J., & Heimbach, P. (2019). Global reconstruction of historical ocean heat storage and transport. *Proceedings of the National Academy of Sciences of the United States of America*, *116*(4), 1126–1131. https://doi.org/10.1073/pnas.1808838115

Zelinka, M. D., Myers, T. A., McCoy, D. T., Po-Chedley, S., Caldwell, P. M., Ceppi, P., et al. (2020). Causes of higher climate sensitivity in CMIP6 models. *Geophysical Research Letters*, *47*(1), 1–12. https://doi.org/10.1029/2019GL085782